Deconvolution of Compton Scatter in SPECT

Carey E. Floyd, Jr., Ronald J. Jaszczak, Kim L. Greer, and R. Edward Coleman

Department of Radiology, Duke University Medical Center, Durham, North Carolina

A deconvolution algorithm has been developed which compensates for Compton scattering in SPECT images. Compton scatter is modeled as a convolution of the nonscattered projection data with an exponential function. Deconvolution of the total (scatter + nonscatter) projection data yields compensated true projection. Using Monte Carlo methods, the scattered and nonscattered components of a SPECT image are simulated thus allowing a comparison of scatter compensated results with direct nonscatter results. The quality of the compensation is evaluated by comparing the ratio of total to direct counts with the ratio of compensated to direct counts. This deconvolution technique has been developed and evaluated for experimentally acquired SPECT data as well as for simulated data.

J Nucl Med 26:403–408, 1985

A primary objective of single photon emission computed tomography (SPECT) is the quantitative localization of radiopharmaceutical distributions within the body. One significant obstacle to accurate SPECT quantitation is the presence of scattered events in the reconstructed image (*1*,*2*). While the scatter contribution may be decreased by an adjustment of energy windows in the SPECT apparatus, the scatter cannot be eliminated. Thus we propose a deconvolution algorithm that provides quantitative scatter compensation. The algorithm requires only a modification to the Fourier frequency filter normally used in the filtered backprojection.

Several algorithms have been proposed for scatter compensation in emission computed tomography (ECT) (*3*–*9*). The deconvolution compensation, based on functional characterization of the scatter component, is similar to one suggested for positron emission tomography (PET) (*8*), but differs significantly from a technique recently presented for scatter compensation in SPECT (*9*). The deconvolution technique (more accurately described as a convolution-subtraction technique) previously described (*9*) requires (a) a convolution to generate an estimate of the scatter and then (b) a subtraction of the estimate from the acquired projections. The technique presented here does not require the subtraction step but instead can be implemented as a modification of the filter used in the backprojection.

Received July 30, 1984; revision accepted Jan. 22, 1985.

For reprints contact: Carey E. Floyd, PhD, Box 3949, Duke University Med. Ctr., Duke University, Durham, NC 27710.

METHODS

With the assumption that Compton scatter may be modeled as a convolution of the nonscattered projection data with an exponential function, deconvolution of this function from the total (scatter + nonscatter) data yields the compensated true data. To determine the parameter values for the exponential function, a Monte Carlo simulation was performed yielding separately a nonscatter and a scatter image for SPECT acquisition of a line source with radius 0.25 cm, length 11.0 cm, in a water filled phantom with radius 11.0 cm, length 11.0 cm. Results obtained using line-source data are significant since the one-dimensional (single slice) projection response to a line source is equivalent to the system response to an impulse function. It follows that the system response to any arbitrary source distribution may be represented as a linear combination of the system response to line sources. This follows from the fact that SPECT is a linear systems process. Thus, for compensation techniques involving linear operations (such as the deconvolution described below) validation of the technique for line-source data should be sufficient so long as the SPECT acquisition represents a linear and shift-invariant process. The phantom dimensions were chosen to duplicate dimensions used in actual experiments. SPECT scans were simulated with the line source in two

different locations: one on the axis of rotation and the other 5.0 cm off-axis but parallel to the axis of rotation.

Description and validation of the Monte Carlo model of SPECT has been presented elsewhere (*10–12*). To justify the assumption that scatter can be modeled as the convolution of the nonscatter projection with an exponential function, this convolution was compared with the Monte Carlo simulated scatter projection. The parameter values in the exponential function were adjusted to match the convoluted profile to the scattered profile. With the parameter values determined, the deconvolution is performed on the total (scatter + nonscatter) projections.

Theoretical development of this deconvolution technique is presented here.

Define: (a) D(x) as the Direct (nonscattered) projection distribution including only photons which have not scattered; (b) S(x) as the Scatter projection distribution including only photons which have scattered in the body (phantom) before detection; (c) T(x) as the Total projection distribution = D(x) + S(x), where T(x) is the projection which would be detected by the SPECT system. Then, assuming that scatter can be represented as the convolution of the direct projection with some smearing function G(x),

$$S(x) = D(x) * G(x)$$

$$T(x) = D(x) + S(x)$$

$$= D(x) + D(x) * G(x)$$

$$= D(x) * (\delta(x) + G(x)),$$

where δ is the Dirac delta functional.

Express in terms of Fourier transforms:

$$FT[T(x)] = FT[D(x)]\ FT[\delta(x) + G(x)],$$

where FT is the Fourier transform operator.

$$D(x) = Ft^{-1}\left[\frac{FT\,(T(x))}{FT\,(\delta(x) + G(x))}\right],$$

which yields the direct nonscattered projections in terms of the total (measured) projection and a smearing function G(x).

When plotted on semilogarithmic coordinates, the projection of the line source shown in Fig. 1 (upper) has tails which are nearly straight lines. The scatter events are shown in Fig. 1 (lower). This step emphasizes the importance of Monte Carlo simulation in the development of scatter compensation algorithms since the scatter events acquired in the photopeak window cannot be experimentally distinguished from the total acquired events. The shape as well as the magnitude of the scatter contribution depends on the energy window used in the SPECT acquisition. Profiles are shown for 5%, 10%, 20%, and 30% full width at half maximum (FWHM)

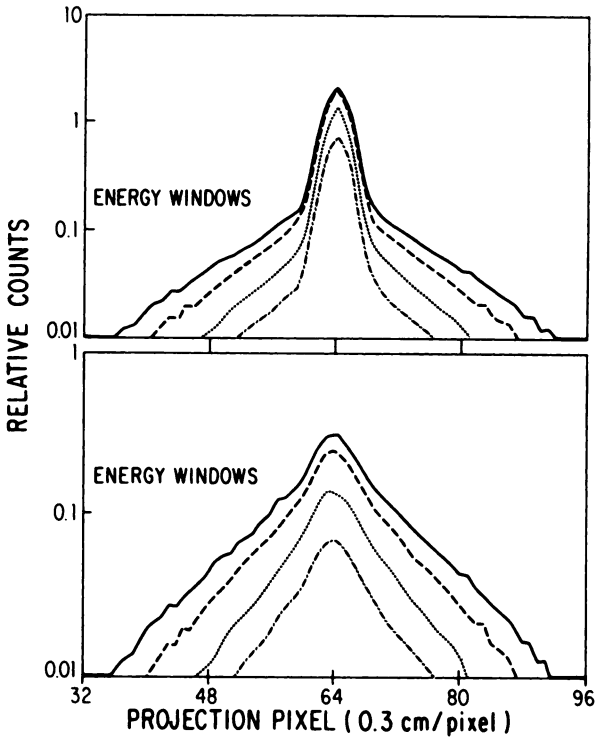

FIGURE 1
Simulated projection profiles for line source in water phantom acquired in four different energy windows: (• – •) 5% (136–144 keV); (• • •) 10% (133–147 keV); (– – –) 20% (126–154 keV); (—) 30% (119–161 keV). Top: Scatter + nonscatter. Bottom: Scatter only

energy windows centered at 140 keV. If the true line spread shape resembles an impulse function, and that the spread of the tails is attributed to Compton scatter, then Compton scatter may be modeled as a convolution of the nonscattered projection data with an exponential function of the form

$$G(x) = \alpha \exp(-\beta|x|)$$

where α and β are parameters. Fitting the exponential convolution to the Monte Carlo simulated scatter component of a line source in the water filled phantom (radius 11 cm, length 11 cm, energy window 126–154 keV, slice thickness 2.5 cm) yields $\alpha = 0.023$ and $\beta = 0.46$ cm^{-1}. Deconvolution of the total (scatter + nonscatter) data yields the compensated true data:

$$D(x) = FT^{-1}\left[\frac{FT\,(T(x))}{FT\,(\delta(x) + 0.023 \exp(-0.46\,|x|))}\right]$$

In our implementation of filtered backprojection, the Fourier Transform of the projections are multiplied by a spatial frequency filter H(f) (which has the form of a ramp multiplied by a generalized Hanning window), described in Ref. (*13*), and the inverse transform is taken of this product. The resulting filtered projections are backprojected to form an image. To implement the

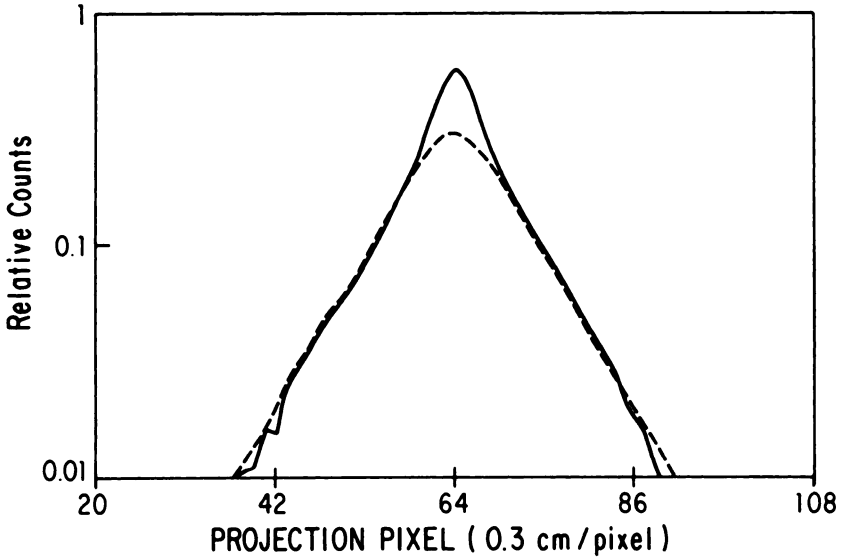

FIGURE 2
Simulated projection profile of scatter component (—) compared with exponential convolution of nonscatter component with exponential function (- - -). Line source in water phantom acquired in 20% (126–154 keV) energy window

scatter deconvolution, the spatial frequency filter H(f) is divided by the Fourier transform of the exponential function. Thus the new spatial frequency filter is given by H(f)/C(f) where

$$C(f) = FT\,[\delta(x) + \alpha \exp(-\beta|x|)].$$

This filter C(f) will be spatially invariant over regions where the density of the scattering medium is uniform. There will be difficulties with the regions near the edges of the body.

RESULTS

The validity of representing the scatter component by convolution of the nonscattered projection with an exponential function is demonstrated for the restricted geometry (described above) by comparing a simulated scatter projection with the convolution of a simulated nonscattered projection with an exponential function as shown in Fig. 2. Fitting the exponential convolution to the simulated scatter component of a line source in a water filled phantom yields $\alpha = 0.023$ and $\beta = 0.46\ cm^{-1}$. Monte Carlo modeling was used to simulate the scatter and nonscatter contributions to the projection data for imaging a line source located at two positions in a cylindrical water phantom. Comparison of reconstructed images of line source in water phantom both on-axis (Fig. 3) and 5 cm off-axis (Fig. 4) reveals a good agreement between the simulated direct projection and the compensated projection. The agreement is less obvious in the off-axis case (Fig. 4) partially due to the poorer statistics in the off-axis simulation. The quantitative accuracy of the compensation is shown by comparing the ratio of total counts to direct (nonscatter) counts with the ratio of compensated counts to direct counts listed in Table 1. The total-to-direct ratio would

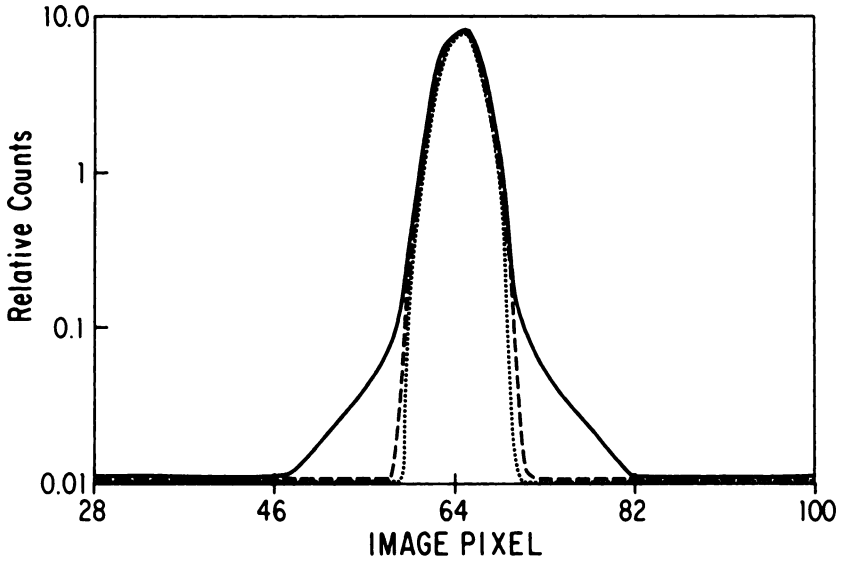

FIGURE 3
Radial slice through reconstructed image of line source 5 cm off axis in water phantom. (—) Total (scatter + nonscatter) data; (- - -) Deconvolution compensated; (• • •) Nonscattered component

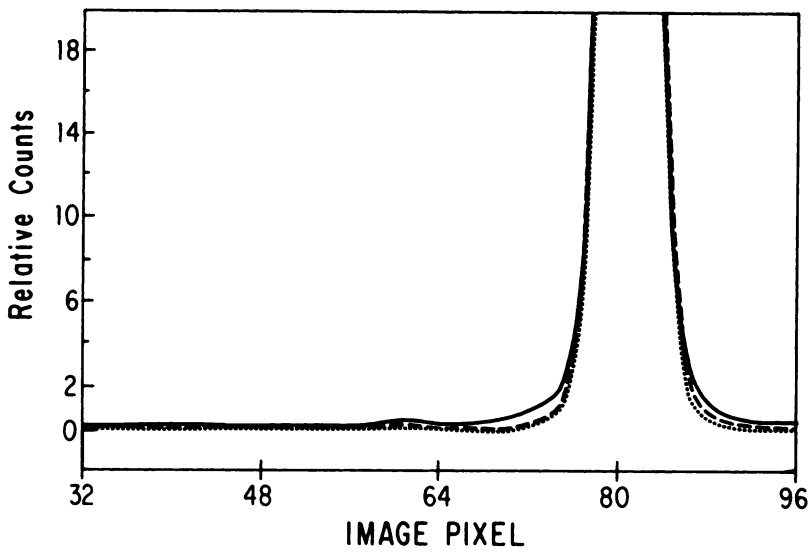

FIGURE 4
Radial slice through reconstructed image of line source on axis in water phantom (—) Total (scatter + nonscatter) data; (- - -) Deconvolution compensated; (• • •) Nonscattered component

be 1.00 for no scatter contribution. The compensated-to-direct ratio would be 1.00 for ideal compensation. Results in Table 1 demonstrate good compensation for this limited test geometry.

With the encouraging results obtained for the limited (but well understood) test geometry, we turn to evaluation of experimental SPECT acquisitions. Three SPECT studies were compensated for scatter using the algorithm and parameters which were developed using the simulation study. First, five line sources were scanned in the water phantom and compared to the same line sources scanned in air. The scan in water was reconstructed using a filtered back projector with a Hanning window cutoff at the Nyquist frequency. Attenuation compensation was performed using the zero order Chang algorithm with an attenuation coefficient value of 0.15. The performance of the scatter compensation may be evaluated by comparing slices through the reconstructed images in Fig. 5. A radial slice is shown in A at the top of Fig. 5, while a tangential slice is shown in B at the bottom. The solid line shows the noncompensated scan in water, the dashed line shows the deconvolved scan in water, while the dotted line shows the scan in air. While complete recovery of the resolution in air is not obtained, the improvement is significant. Quantitatively, the ratio of total counts (air/water) was improved from 0.76 for no compensation, to 0.98 for the compensated image (1.00 for ideal compensation). The second study reconstructed a 6.3-cm-diam cold sphere immersed in an 22-cm-diam active cylindrical phantom. The compensated image is shown at right in Fig. 6 with the noncompensated image on the left. The increase in contrast for the compensated image is apparent. A quantitative evaluation for this phantom is provided by examining the contrast factor defined by

$$C_f \frac{R - B}{B}$$

where R is the mean value per pixel in the region of interest and B is the mean value per pixel in a background region. For the noncompensated image, $C_f = -0.76$. For the compensated image, $C_f = -0.88$ showing a marked improvement due to scatter reduction in the cold region. This result is significant for a case where there is expected to be considerable scatter contribution from other image planes. Third, a clinical image of a liver having a cold lesion defect is presented in Fig. 7 with the deconvolved image on the right, no compensation on the left. An improvement in lesion contrast is apparent in this clinically common geometry.

DISCUSSION AND CONCLUSION

The exponential deconvolution technique of scatter compensation has been demonstrated to yield good quantitative compensation for scatter in several representative geometries. Both line-source resolution as well as contrast factors have been shown to be improved. These results indicate that deconvolution of an exponential function can significantly reduce the effect of

TABLE 1
Ratio of Counts in Reconstructed Images for Line Source at Two Locations*

Ratio	On-axis	Off-axis
Total Direct	1.39	1.32
Compensated Direct	1.04	0.99

* Ratios are Total (scatter + nonscatter) to Direct (nonscatter) and Compensated to Direct. Total to Direct ratio would be 1.00 for no scatter contribution. Compensated to Direct ratio would be 1.00 for ideal compensation.

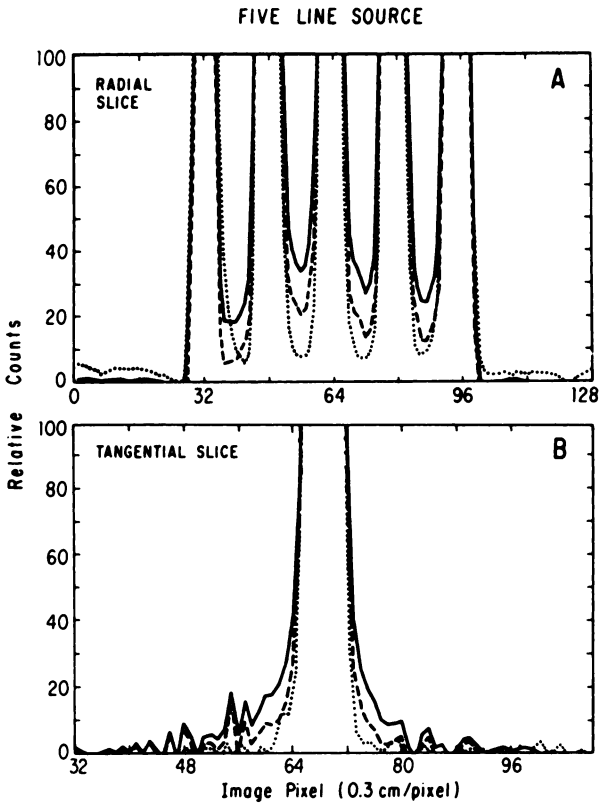

FIGURE 5
Slice through reconstructed image of experimentally acquired five line source. A: Radial slice; B: Tangential slice. (—) Scan in water (scatter + nonscatter) with no compensation; (- - -) Deconvolution compensated; (• • •) Scan in air (no scatter)

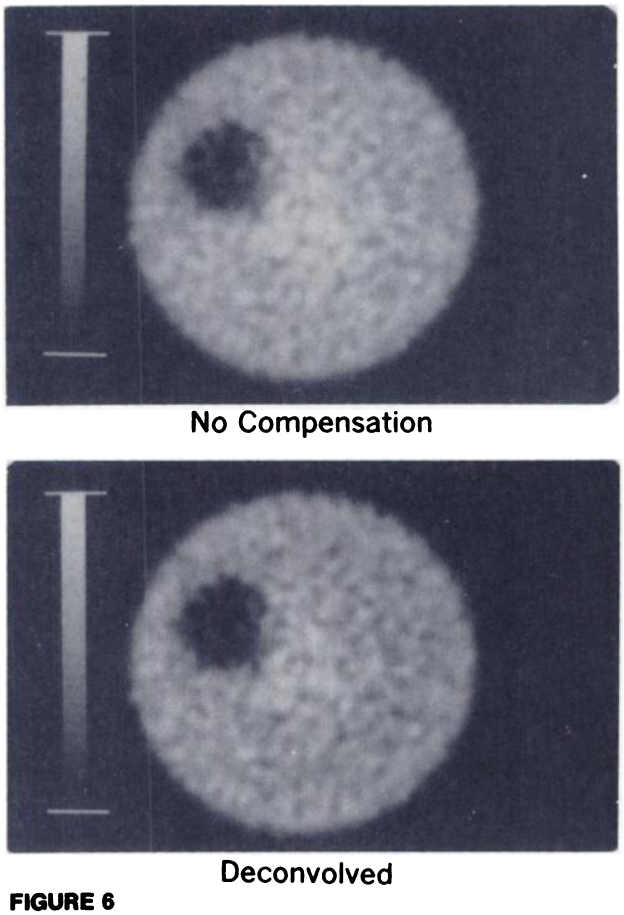

FIGURE 6
Reconstructed image of 6.3-cm-diam cold sphere immersed in 22 cm diam active cylindrical phantom. Noncompensated image at top, compensated at bottom

Compton scattering in quantitative SPECT imaging.

There are several difficulties with the deconvolution compensation technique which will be common to any compensation technique which relies on a functional parameterization of the scatter. The parameterization is dependent on (a) the slice thickness; (b) the energy window used in the acquisition; (c) the detector energy resolution; (d) the density of the scattering medium; (e) the depth of scatter location. Items a–c are acquisition system dependent and usually do not vary significantly from acquisition to acquisition. Item d implies that this algorithm is dependent on having a uniform scattering

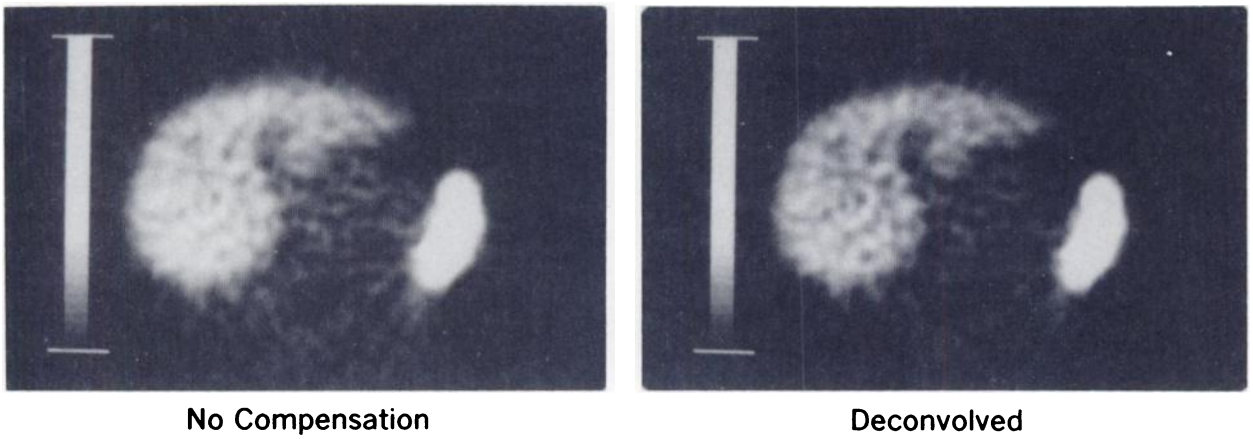

FIGURE 7
Reconstructed liver scan with cold lesion. Noncompensated image at left, compensated at right

medium. Monte Carlo simulation techniques will be used in the future to investigate the strength of this dependence on uniformity and also the problems associated with Item e. While these problems will be investigated in the future, the preliminary results shown indicate that the deconvolution algorithm, using parameters derived from simulation of a simple test geometry, can quantitatively improve resolution and contrast in SPECT acquisitions. The development of the algorithm assumes that there is some nonscattered component in reconstructed slice. In SPECT acquisition, there can be slices in which there will be scattered events but no nonscattered events. This interplane scatter will not be reduced by the present algorithm, but will require a full three-dimensional reconstruction with two-dimensional deconvolution (across the full detector field of view) at each angular projection.

We suggest that this deconvolution technique is a fast, practical approach to scatter compensation while we await the full development of unified reconstruction algorithms, such as Inverse Monte Carlo (*14*), which simultaneously include compensation for scatter, attenuation, and depth dependent collimator resolution.

ACKNOWLEDGMENTS

This investigation was supported in part by PHS grant number CA33541 awarded by the National Cancer Institute, DHHS. The authors are grateful to Siemens Gammasonics, Inc. for partial support of their SPECT system.

REFERENCES

1. Keyes JW: Perspectives on tomography. *J Nucl Med* 23:633-640, 1982
2. Budinger TF: Physical attributes of single-photon tomography. *J Nucl Med* 21:579-582, 1980
3. Logan J, Bernstein HJ: A Monte Carlo simulation of Compton scattering in positron emission tomography. *J Comput Assist Tomogr* 7:316-320, 1983
4. Pang SC, Genna S: The effect of Compton scattered photons on emission computed transaxial tomography. *IEEE Trans Nucl Sci* NS-26:2772-2774, 1979
5. Jaszczak RJ, Greer KL, Floyd CE, et al: Improved SPECT quantitation using compensation for scattered photons. *J Nucl Med* 25:893-900, 1984
6. Bergstrom M, Erikson L, Bohm C, et al: Correction for scattered radiation in ring detector positron camera by integral transformation of the projections. *J Comput Assist Tomogr* 7:42-50, 1983
7. Egbert SD, May RS: An integral-transport method for Compton-scatter correction in emission computed tomography. *IEEE Trans Nucl Sci* NS-27:543-557, 1980
8. King PH. Hubner K, Gibbs W, et al: Noise identification and removal in positron imaging systems. *IEEE Trans Nucl Sci* NS-28:148-151, 1981
9. Axelsson B, Msaki P, Israelsson A: Subtraction of Compton-scattered photons in single photon computerized tomography. *J Nucl Med* 25:490-494, 1984
10. Floyd CE, Jaszczak RJ, Harris CC, et al: Energy and spatial distribution of multiple order Compton scatter in SPECT: A Monte Carlo investigation. *Phys Med Biol* 29:1217-1230, 1984
11. Beck JW: Analysis of a camera based single photon emission computed tomography (SPECT) system. PhD Dissertation, Duke University, (University Microfilms), Ann Arbor, Michigan, 1982
12. Beck JW, Jaszczak RJ, Coleman RE, et al: Analysis of SPECT including scatter and attenuation using sophisticated Monte Carlo modeling methods. *IEEE Trans Nucl Sci* NS-29:506-511, 1982
13. Jaszczak RJ, Coleman RE, Whitehead FR: Physical factors affecting quantitative measurements using camera-based single photon emission computed tomography (SPECT). *IEEE Trans Nucl Sci* NS-28:69-80, 1981
14. Floyd CE, Jaszczak RJ, Coleman RE: Inverse Monte Carlo: A unified reconstruction algorithm for SPECT. *IEEE Trans Nucl Sci* NS-32:1985: in press